

THE INTERNATIONAL SOCIETY OF
PRECISION AGRICULTURE PRESENTS THE
13th INTERNATIONAL CONFERENCE ON
PRECISION AGRICULTURE

July 31-August 4, 2016 • St. Louis, Missouri USA

Towards Calibrated Vegetation Indices from UAS- derived Orthomosaics

Klaas PAULY

Unmanned Aircraft Systems, Trimble Navigation Ltd., Gent (Belgium)

**A paper from the Proceedings of the
13th International Conference on Precision Agriculture
July 31 – August 4, 2016
St. Louis, Missouri, USA**

Abstract. *Crop advisors and farmers increasingly use drone data as part of their decision making. However, the vast majority of UAS-based vegetation mapping services support only the calculation of a relative NDVI derived from compressed JPEG pixel values and do not include the possibility to include more complex aspects like soil correction. In our ICPA12 contribution, we demonstrated the effects and consequences of the above shortcomings. Here, we present the stepwise development of a solution to ensure reliable input for crop advisors as a basis for site-specific crop management based on drone data. UAS flights are executed with a Trimble UX5 (HP) over a Belgian farm comprising four different crop types during a 3 month interval. Vegetation index maps derived from compressed JPEG imagery as well as preprocessed raw sensor data from a modified conventional CIR camera are evaluated against those from a true multispectral camera, and we examine the ability to calibrate the maps. Resulting maps are compared to NDVI values from the active close-range Trimble GreenSeeker crop sensor. Based on the results, we discuss under which conditions the three different data types can be used to complement traditional measurements in addressing within-season crop variability.*

Keywords. UAS, Trimble UX5, CIR, JPEG, RAW, multispectral, NDVI.

The authors are solely responsible for the content of this paper, which is not a refereed publication.. Citation of this work should state that it is from the Proceedings of the 13th International Conference on Precision Agriculture. EXAMPLE: Lastname, A. B. & Coauthor, C. D. (2016). Title of paper. In Proceedings of the 13th International Conference on Precision Agriculture (unpaginated, online). Monticello, IL: International Society of Precision Agriculture.

Introduction

In a changing world, farmers are required to adopt more precise and flexible techniques to address the rising population, environmental stress and climate change (Wezel et al., 2014; Zarco-Tejada et al. 2014a). Crop scientists, consultants and growers increasingly turn to remote sensing tools to provide guidance in where and when efficiency can be improved (Mulla, 2013). Recently launched satellite constellations provide free or relatively cheap input for large scale, high resolution and high-frequency services, sparking a revolution in the availability of information (e.g. Aschbacher and Milagro-Pérez, 2012; Tyc et al., 2005). Additionally, unmanned aircraft systems (UAS) attract growing interest to fill the gaps in information if resolution requirements or weather conditions exclude the use of spaceborne or manned airborne platforms (Zhang and Kovacs, 2012). Some unmanned applications in precision agriculture successfully build directly on years of progress in UAS photogrammetry. Examples include the generation of precisely georeferenced orthomosaics for early site-specific weed management (Gómez-Candón et al., 2014) and 3D models for drainage, erosion and plant height monitoring (Bendig et al., 2014; d'Oleire-Oltmanns et al., 2012; Zarco-Tejada et al., 2014b). On the other hand, even though commercial online crop vigor mapping services are booming, the application of multispectral remote sensing algorithms on UAS imagery has proven more challenging (Pauly, 2014).

In the early years of commercial availability of UAS (2009 – 2014), true multispectral cameras with discrete, narrow bands were too big and too expensive to routinely mount in small systems, especially in fixed wing systems. Instead, researchers and manufacturers turned to small commercial off-the-shelf (COTS) cameras to meet the demand for imagery of large agricultural fields at very high resolution. The spectral characteristics of digital sensors with a Bayer RGB color filter array (CFA) were exploited to generate color-infrared (CIR) images through the use of specific filter adaptations (e.g. Hunt et al., 2010). Several commercial UAS providers and some research publications used the term “multispectral” for these modified COTS cameras, causing some confusion about the data type and quality in the drone operator community inexperienced in remote sensing. At the same time, research papers also highlighted the shortcomings of CIR imagery from COTS cameras in remote sensing analyses. These concerns focused mainly on the influence of vignetting and angular variations in reflectance when analyzing single images or orthomosaics generated with low sideward overlap (Lebourgeois et al., 2008; Lelong et al., 2008; Rasmussen et al., 2016), and on JPEG compression artefacts versus linear uncompressed RAW sensor data (Lebourgeois et al., 2008; Lebourgeois et al., 2012; Verhoeven, 2010). Issues caused by vignetting and angular variations can be easily solved by applying a flat field correction and using very high overlap (> 80 %) both in the forward and sideward direction, which also significantly improves vertical accuracy of the 3D models (Pauly, 2016). While some studies in specific conditions showed only marginally better results from processing RAW imagery (Lebourgeois et al., 2008), consensus is growing that the RAW format should be preferred over JPEG for quantitative analyses when working with COTS cameras. This is because RAW pixel digital numbers (DN) show a linear response to radiant energy, as opposed to gamma compressed JPEG DN (Pauly, 2014; Verhoeven, 2010). However, adoption of RAW processing has remained low due to the (perceived) complexity and very high data storage and computing capacity requirements. Additionally, the issue of spectral band contamination due to the broad and overlapping response of the Bayer CFA filters in both JPEG and RAW data from COTS cameras received much less attention. Although the use of notch filters and linear band recombinations have been proposed to cope with the spectral contamination, the issue remains largely unaccounted for (Berra et al., 2015; Pauly, 2014; Rabatel et al., 2014; Verhoeven, 2010).

Over the last two years, commercial narrowband multispectral cameras have been sufficiently decreased in size and cost to be considered a better solution for quantitative image analysis even in fixed wing UAS. While many studies using similar camera setups have already demonstrated the benefits of their spectral data quality on retrieving biophysical crop information, some drawbacks such as the reduced spatial resolution remain (e.g. Fang et al., 2016; Peña et al., 2015). However, a clear comparison of the three imagery types used in UAS-based precision agriculture (JPEG versus

RAW from COTS cameras, versus true multispectral imagery) and the implications on the resulting vegetation index (VI) maps has not been published.

This study aims to disentangle the effects of compression artefacts and spectral contamination in COTS cameras as compared to true narrowband multispectral imagery, and evaluate the benefit of spatial versus spectral resolution. We look at the data in spectral space to understand the different outcomes of commonly used vegetation indices, and discuss the extent to which spectral data can be improved by using soil correction, along with the possibility to use VI maps in multi-temporal analyses. Rather than attempting to correlate the resulting VI maps with specific biophysical traits of the crops, we want to compare similar measurement types obtained from airborne and ground-based data. Ultimately, our goal is to advise on the best suited application for each data type.

Materials and methods

Data acquisition

Flight operations were carried out on 17 February, 20 April and 27 May 2016 in clear sky conditions over 25 ha of the Trimble UAS test site in Assenede (Belgium). The test site consists of farmland with grass pastures and uniformly managed winter wheat, maize and flax fields next to some built up areas with access roads. Each flight day, the area was covered by a Trimble UX5 equipped with a MicaSense RedEdge 3 set to capture 80% forward and sideward overlap at 120 m above ground level (AGL), resulting in a ground sample distance (GSD) of 8.2 cm. During the February and April flight days, a Trimble UX5 HP equipped with a modified color-infrared (CIR) Sony a7R fitted with a 15 mm lens also covered the area at 85 % forward and sideward overlap and at a height of 120 m AGL, resulting in a GSD of 3.9 cm. The orientation of the UX5 and UX5 HP flight lines was identical and time between both flights was kept to a minimum. The UX5 HP CIR datasets also included pre- and post-flight images of the MicaSense reflectance calibration panel.

On each flight day, roughly 100 ground-based normalized difference vegetation index (NDVI) measurements were collected with the Trimble GreenSeeker HandHeld at a constant height of 80 cm above the target, of which the center point was georeferenced to 2 cm accuracy using a Trimble R8 RTK GNSS system. GreenSeeker NDVI measurements were collected over all relevant terrain and cover types. This allowed UAS data to be compared to a commonly used form of crop vigor and nitrogen status data as input for site-specific crop management.

Image processing

The MicaSense RedEdge imagery was captured in auto exposure mode and stored in camera as 12 bit linear uncompressed TIFF files. For each of the five bands per acquisition point, the camera stores a single 1.2 MP image in a 2.3 MB file. All datasets, including pre- and post-flight images of the reflectance calibration panel offered with the camera was uploaded to the MicaSense Atlas cloud processing service, which includes pre-processing steps such as vignetting correction and takes exposure parameters into accounting when converting to reflectance. The cloud engine returns 5-band 16 bit per band linear losslessly compressed geoTIFF orthomosaics with DN scaled to reflectance for the blue (B), green (G), red (R), red edge (RE) and near-infrared (NIR) parts of the electromagnetic spectrum.

The Sony a7R was modified by removing the internal NIR-blocking filter and using an external Schneider Optics 040 longpass filter with a cut-on at 530 nm, resulting in 3-band R-G-NIR imagery. In this configuration, pixels covered by a blue filter in the Bayer CFA receive only NIR, while pixels covered by green and red filters receive mostly visible green or red, together with some of the red edge and NIR. The CIR camera was set to store 36 MP 3-band 14 bit per band linear lossy compressed RAW files (35 MB each, in Sony's proprietary ARW format) simultaneously with 36 MP 3-band 8 bit per band gamma-compressed JPEG files, roughly 15 MB each. Figure 1 shows the

camera response graphs for the MicaSense RedEdge in comparison to the Sony a7R CIR camera set in RAW and JPEG

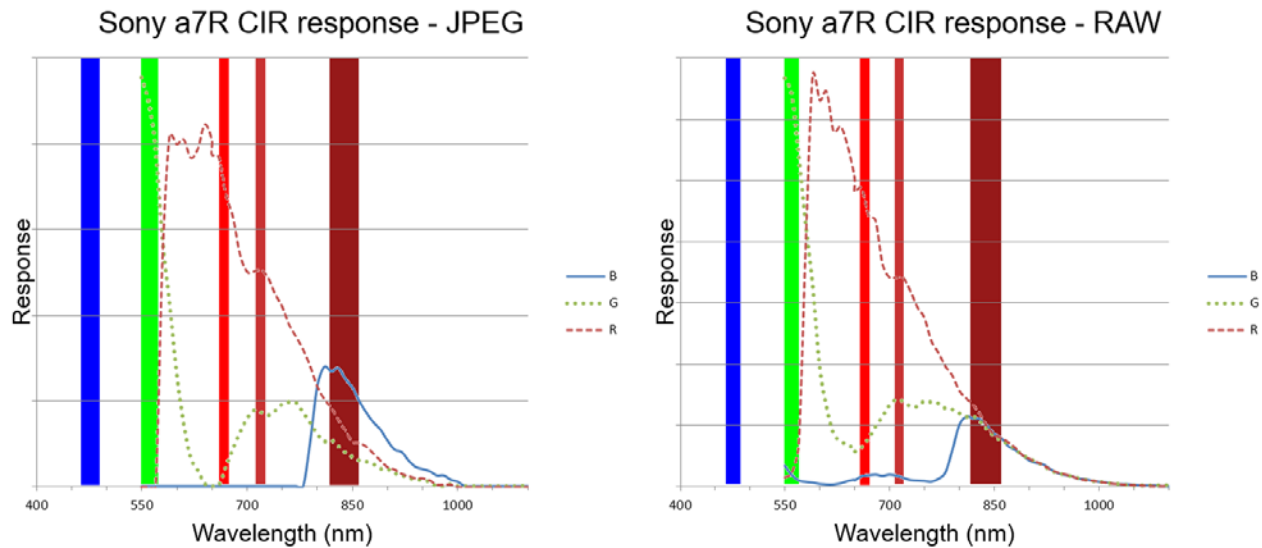


Figure 1. Spectral response of the Trimble UX5 HP Sony a7R modified CIR camera in JPEG (left) and RAW (right). The spectral response of the MicaSense RedEdge blue, green, red, red edge and NIR bands is shown in overlay blocks.

modes, respectively, obtained through analysis of the camera with a monochromator as described in Verhoeven (2009). A custom camera white balance was set by pointing the camera together with the external filter to a white target, resulting in image colors representative of the physical light acquisition (with vegetation in blue tints due to NIR primarily captured by the blue pixels in the CFA). A fixed exposure program was selected (constant shutter speed, aperture and ISO value throughout the flight) to ensure a simple relation between radiant energy and pixel DN in the resulting orthomosaics.

Following a flat-field correction in Trimble Access Aerial Imaging, images in JPEG format were directly processed in accordance with standard practice in Trimble UASMaster 7.1 (Pauly, 2016). This includes using precise post-processed GNSS solutions for the camera positions as input for the geometric camera calibration and a single ground control point to ensure a pixel-level horizontal fit of the orthomosaic to all ground control points in the area of interest. RAW files were first converted to 3-band 16 bit per band linear uncompressed TIFF files in RawTherapee 4.2.1, 200 MB each (using the ddraw engine; Coffin, 2008). The VNG4 demosaicing algorithm was used to account for color crosstalk caused by the specific combination of a wide angle lens and the relatively thick sensor cover glass on the digital full frame sensor in the Sony a7R. The conversion also included flat field correction to correct for vignetting and color shift. The camera white balance was applied while all other correction and enhancement algorithms were disabled, largely corresponding to the methodology described by Verhoeven (2009). The TIFF files were then processed into 3-band 16 bit per band linear uncompressed geoTIFF orthomosaics, similar to the JPEG image processing in Trimble UASMaster 7.1. Although the pixel DN in the TIFF orthomosaics resulting from this process were uniformly and linearly related to radiant energy, they were not scaled to reflectance. In an attempt to calibrate the orthomosaic TIFF from RAW processing post-hoc to reflectance, the orthomosaic DN were divided by an average DN value obtained from the pre- and post-flight RAW images of the MicaSense reflectance calibration panel per band.

Analysis of the orthomosaics

All data layers were imported in ESRI ArcGIS 10.4 and pixel-level alignment of all data layers including ground measurements was ensured prior to analysis. Since the MicaSense Atlas cloud

does not include ground control points during the adjustment, the resulting orthomosaics were initially shifted in relation to the UX5 HP orthomosaics and ground measurement data. Therefore, a one-click automatic registration to the UX5 HP data using a second order transformation was applied to the MicaSense orthomosaics in ArcMap prior to analysis. For each orthomosaic, the NDVI was calculated based on the pixel DN. For the February orthomosaics, the TSAVI was also calculated by extracting NIR and R pixel DN for a sample of 2500 bare soil points to derive the soil line slope and intercept values. Ensuring proper matching of the GreenSeeker HandHeld measurement footprints with the pixel extents in the vegetation index maps, VI values were extracted from all generated maps for the relevant GreenSeeker measurement points. Additionally, for the April orthomosaics, NIR and R pixel DN were extracted at a 1 m sampling interval over the entire extent of the scenes and plotted in spectral space to analyze the effect of the different image acquisition and processing techniques on the shape of the so-called tasseled cap feature, important in understanding the relation between image-based VI maps and ground-based NDVI measurements. Table 1 provides an overview of the data types and analyses.

To analyze the reliability of each data type in multitemporal monitoring, UAS-based NDVI values and spectral profiles for three vegetation types (winter wheat, isolated weed plants and grassland) were plotted over time for the available data acquisitions. Pixel DN or NDVI values for ten randomly picked sites per vegetation type were averaged to generate the plots. Additionally, a test was performed to estimate how stable the relation between UAS-based NDVI and ground-based GreenSeeker NDVI measurements are over time. The idea was to check how well UAS-based NDVI maps can serve as replacement or complementary input source to generate variable rate prescription maps based on existing rules. The best fit equations from the February datasets were used as a model to predict ground-based GreenSeeker NDVI measurements from later points in time, with the subsequent UAS-based NDVI values as input. Using the corresponding GreenSeeker NDVI measurements from these later points in time as independent check points, the root mean squared error (RMSE) is reported.

Results and discussion

Data characteristics in spectral space

A first indication on differences in spectral data quality can be obtained through visual inspection of false color composite orthomosaics. Figure 2a shows the difference in color appearance characteristic of orthomosaics derived from modified commercial off-the-shelf CIR cameras as compared to orthomosaics from true narrowband multispectral cameras, with the same level of image display enhancements applied. The CIR orthomosaic looks quite pale and could be described in shades of pink going from bare earth over sparse, emerging crops to dense grass fields.

Table 1. Overview of analyses types on the orthomosaics obtained from different sensors and processing techniques.

| Flight day | Dataset type | Analysis type | Details |
|-------------------------|---------------------------|---------------|--|
| 17 Feb 2016 | Sony a7R R-G-NIR (JPEG) | NDVI | $NDVI = \frac{b3 - b1}{b3 + b1}$ (1) |
| | | TSAVI | $TSAVI = \frac{s \times (b3 - s \times b1 - a)}{a \times b3 + b1 - a \times s + 0.08 \times (1 + s^2)}$ (2) Where s = soil line slope and a = soil line intercept |
| | Sony a7R R-G-NIR (RAW) | NDVI | Same as (1) |
| | | TSAVI | Same as (2) |
| | MicaSense B-G-R-RE-NIR | NDVI | $NDVI = \frac{b5 - b3}{b5 + b3}$ (3) |
| | | TSAVI | $TSAVI = \frac{s \times (b5 - s \times b3 - a)}{a \times b5 + b3 - a \times s + 0.08 \times (1 + s^2)}$ (4) |
| Sony a7R R-G-NIR (JPEG) | NDVI Tasseled Cap plot | Same as (1) | |
| Sony a7R R-G-NIR (RAW) | NDVI | Same as (1) | |

| | | |
|------------------------|---------------------------|---------------------------|
| MicaSense B-G-R-RE-NIR | Tasseled Cap plot NDVI | Same as (3) |
| 27 May 2016 | MicaSense B-G-R-RE-NIR | Tasseled Cap plot NDVI |
| | | Same as (3) |

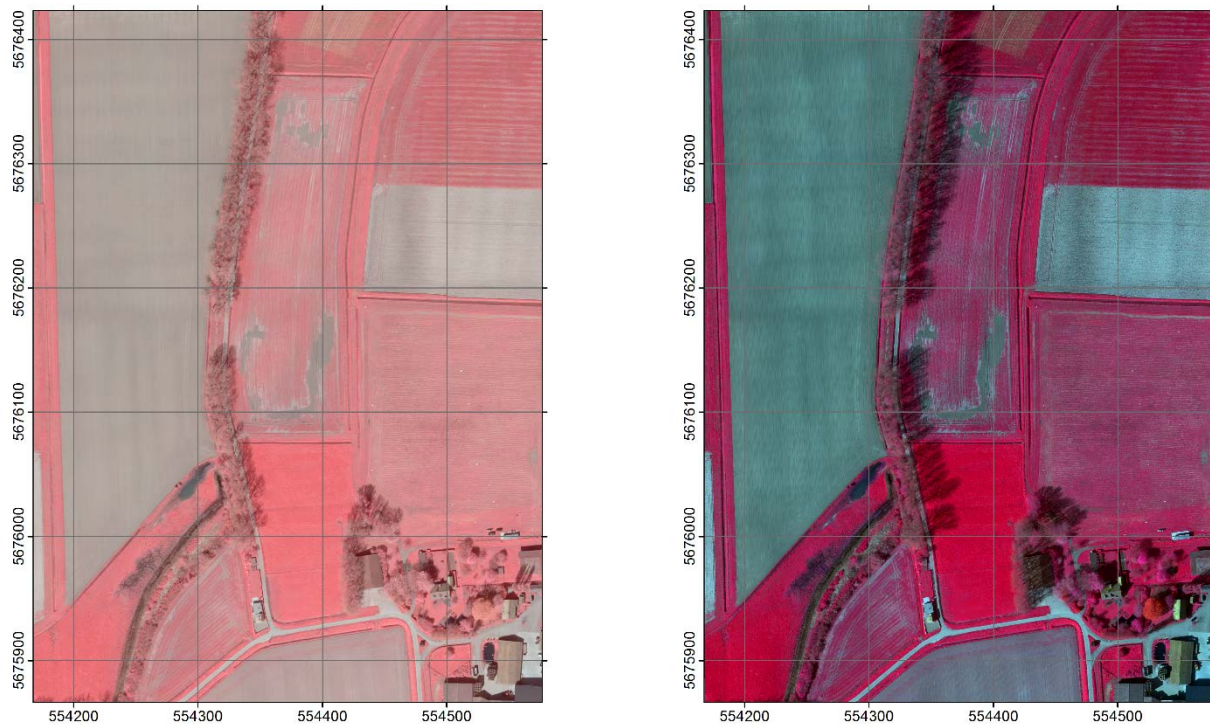


Figure 2a. Left: false color (NIR, R, G) composite orthomosaic from the UX5 HP with CIR camera on 20 April 2016, obtained from RAW processing. Right: false color (NIR, R, G) composite orthomosaic obtained from the UX5 with a true narrowband multispectral camera (MicaSense RedEdge) on 20 April 2016. A 5 standard deviation histogram stretching and gamma factor of 1.5 was applied to all bands for both orthomosaics to enhance visibility in the same way. While the orthomosaic from the UX5 HP with CIR camera obtained from JPEG processing is not shown, it looks very similar in terms of color and tones to the RAW orthomosaic shown on the left, except that no histogram stretching or gamma needs to be applied to get the same appearance.

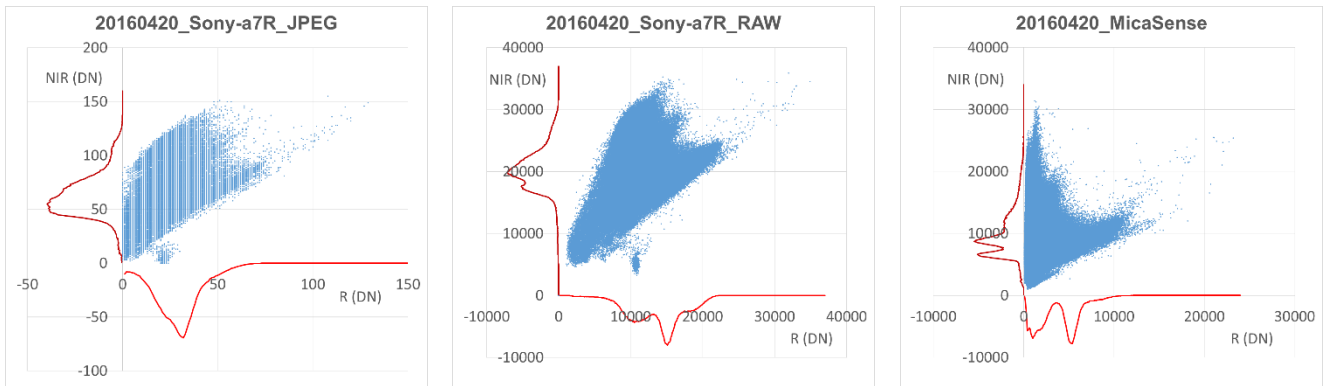


Figure 2b. NIR versus R tasseled cap scatterplots for the entire orthomosaic scene as shown in figure 2a, sampled at 1 m, obtained from CIR JPEG (left), CIR RAW (middle) and true narrowband multispectral (right) image processing. The line graphs at opposite sides of the axes represent the (scaled) frequency distribution of the plotted points along the axis.

In contrast, the multispectral orthomosaic shows markedly distinct colors, from greenish tints of bare earth where much stronger contrasting patterns can be found compared to the CIR orthomosaic, to vivid pure red for dense growth. Although more local contrasts could be enhanced in the CIR

orthomosaic by further stretching the histogram and increasing gamma factors, this always goes at the expense of loss of contrasts in other parts of the orthomosaic. The observation that the difference in appearance is much bigger between CIR and true multispectral false color composites than between JPEG-based and RAW-based CIR orthomosaics, illustrates that the difference is more caused by spectral contamination rather than initial dynamic range or compression artefacts in the processed imagery.

The tasseled cap plots in figure 2b further clarify the influence of gamma compression artefacts in JPEG imagery next to the issue of spectral contamination in CIR cameras in general, regardless of the data type used. In the JPEG graph, data compression artefacts are clearly visible as points plotted on discrete horizontal and vertical lines: because of the relatively few DN values available in an 8 bit range, many NIR values are plotted over the same R value, and vice versa. The RAW-based plot does not show these lines resulting from compression artefacts; there are enough unique (NIR, R) combinations possible to give the plot a continuous rather than a discrete appearance. However, both JPEG and RAW plots are similar in that, although the line of bare soils can be isolated in the higher DN range (> 75 for JPEG or > 25000 for RAW), the shape of the tasseled cap is severely flattened. This is because both bands are highly correlated, with the red band also containing a small but significant portion of NIR light. There is no unique place along the line of bare soils where high NIR points result in the distance away from the line being maximized, an essential feature to get reliable results from vegetation indices, including the NDVI and Kauth-Thomas transformations. As a result, the frequency distribution of DN values is either unimodal in the case of JPEG imagery where spectral contamination is exacerbated by data compression artefacts, or only slightly bimodal in the case of RAW imagery where only spectral contamination is an issue. This means that, especially for sparse growth, the distinction between bare soil and vegetation is much harder to make using the NDVI. In contrast, a typical tasseled cap shape with a unique point where distance away from the bare soil line is maximized for dense, healthy vegetation is found for true narrowband multispectral data. A strongly bimodal frequency distribution in both NIR and red DN is also visible in the true multispectral data plot where neither data compression nor spectral contamination exist, resulting in reliable NDVI values while also allowing for meaningful Kauth-Thomas transformations.

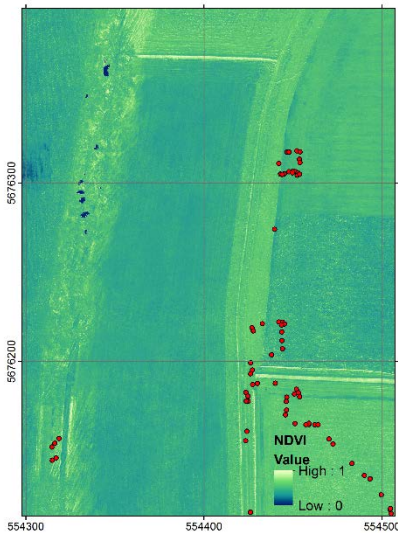
Improving VI maps with soil correction

Although the tasseled cap plots for CIR-based orthomosaics show a difficult distinction between bare soil and vegetation for some growth stages and health statuses in the NDVI, it is still possible to derive the slope and intercept of the bare soil line, mainly relying on higher DN, and to apply some form of soil correction. Overall, the ensemble of points representing bare soil in the plot is broader and includes points that would show up as true outliers for the same sample in the plot of true multispectral data, e.g. in the case of small isolated weed plants. Figure 3 shows that while the expected linear correlation between UAS-based NDVI values and GreenSeeker NDVI measurements is either very poor ($R^2 = 0.28$ in the case of JPEG imagery) or relatively good ($R^2 = 0.82$ in the case of RAW imagery) for CIR data, results are significantly better for both data types when using a distance based, soil-corrected vegetation index such as the TSAVI ($R^2 = 0.82$ for JPEG and $R^2 = 0.93$ for RAW). By contrast, the NDVI from true multispectral data is already highly linearly correlated with GreenSeeker NDVI values ($R^2 = 0.92$). Regardless, results can still be improved by relying on the large distance away from the line of bare soils in the tasseled cap plot for soil correction such as applied in the TSAVI ($R^2 = 0.96$) for the February dataset in this study. The observation that the TSAVI performs overall much better than the NDVI in comparison with ground-based NDVI measurements on UAS-based CIR data during the vegetative growth stages is in accordance with observations made by Pauly (2014). Hence, we believe that soil-corrected vegetation indices should receive more attention and should be adopted more widely for UAS-based in-season monitoring (especially during the early growth stages), even for true multispectral data. Currently, many online image analysis services do not allow for the generation of this type of VI map.

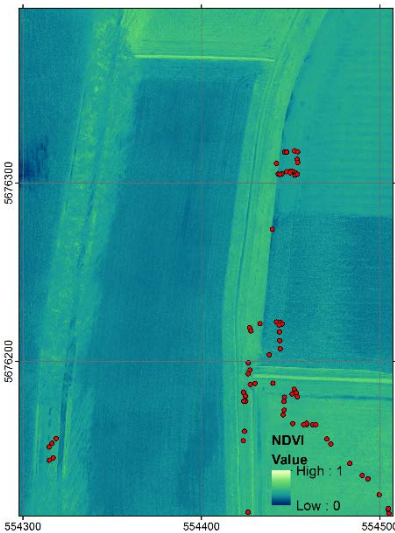
Multitemporal analysis

While a high correlation of UAS-based NDVI values versus ground-based NDVI measurements for a single orthomosaic can mean good quantitative discrimination of vegetative states for that particular scene, it doesn't necessarily mean that UAS-based NDVI maps are therefore also consistent over time. Some UAS-based data types are inherently difficult or impossible to calibrate over time, especially when DN values have no linear relation to radiant energy, e.g. with JPEG data. In this case, the UAS-based NDVI should be referred to as a relative NDVI, rather than a true (absolute) NDVI.

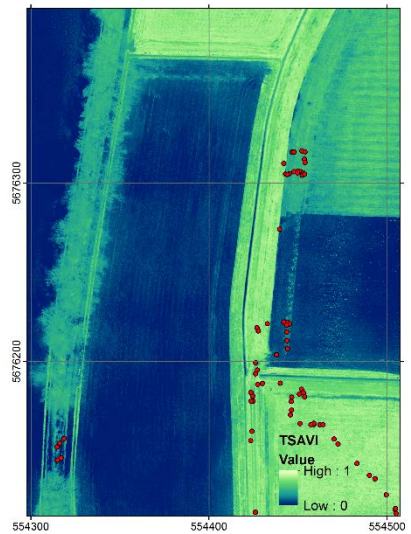
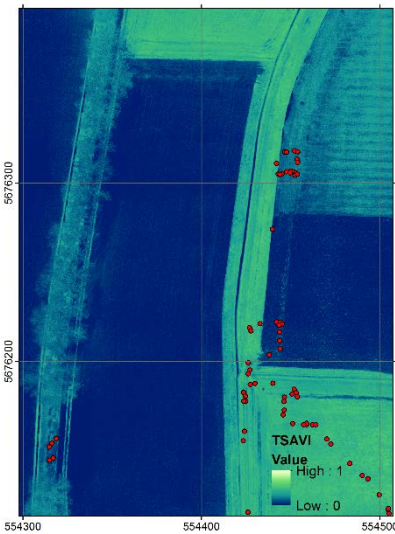
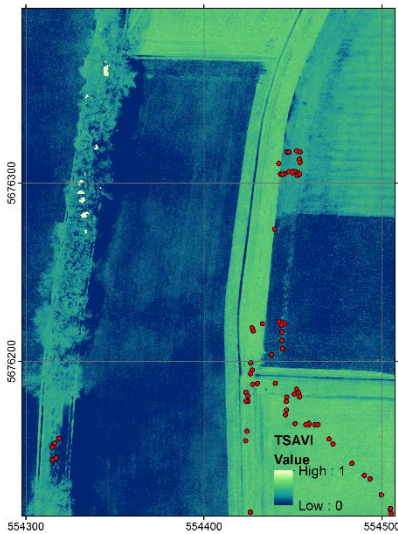
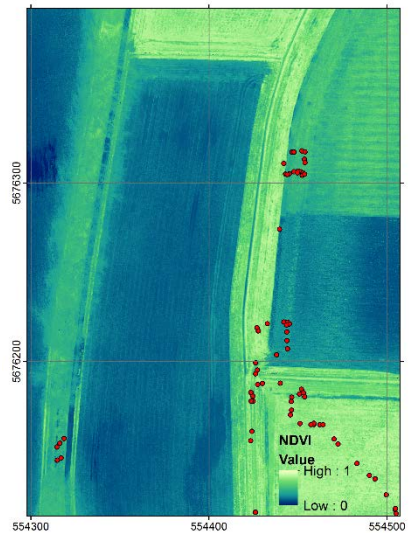
20160217_Sony-a7R_JPEG



20160217_Sony-a7R_RAW



20160217_MicaSense



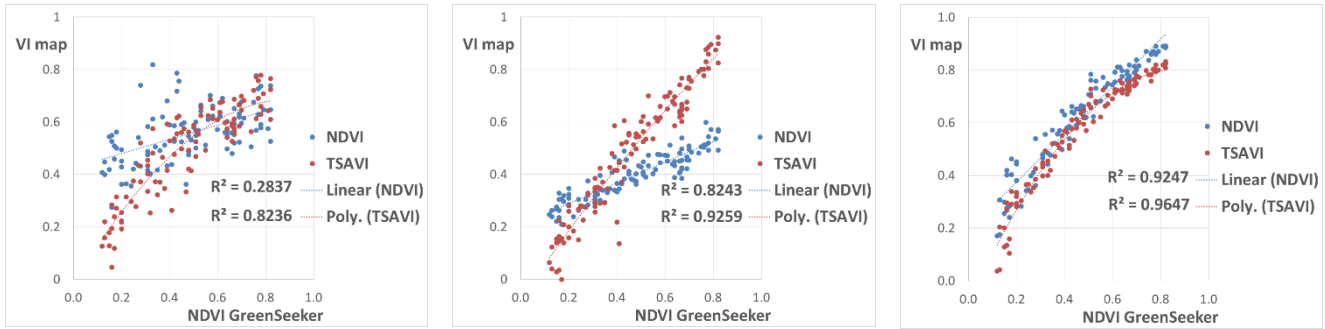


Figure 3. Comparison of VI maps (extract shown) for the three different image processing techniques: JPEG imagery from a CIR camera (left), RAW imagery from a CIR camera (middle) and true narrowband multispectral imagery (right). Upper row: NDVI, middle row: TSAVI. Red dots on the maps represent ground-based GreenSeeker NDVI measurement points. The lower row shows the correlation between UAS-based NDVI (blue) and TSAVI (red) values and ground-based GreenSeeker NDVI values.

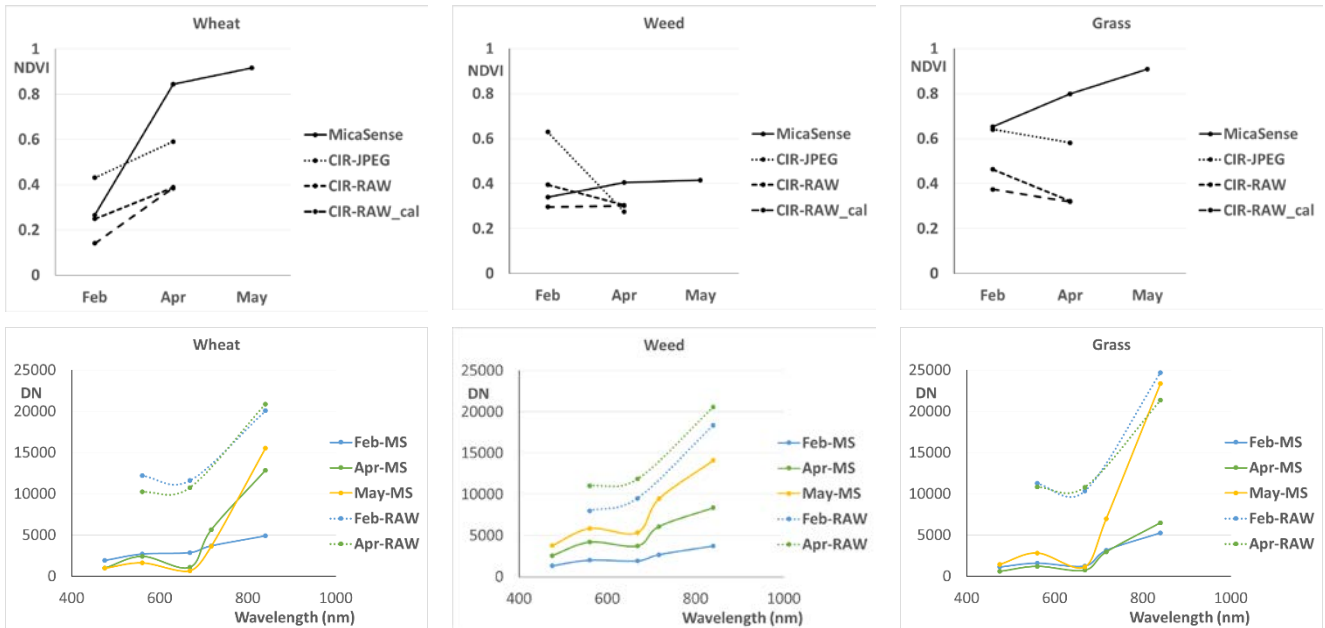


Figure 4. Multitemporal analysis of NDVI values (top row) and spectral profiles (bottom row) for three vegetation types (wheat, left; isolated weed plants, middle; permanent grassland, right) according to the different image processing techniques. RAW-cal = orthomosaic derived from RAW image processing and calibrated post-hoc for reflectance using images of the MicaSense reflectance calibration panel; MS = true narrowband multispectral.

Figure 4 (top row) shows the evolution in UAS-based NDVI values for three different vegetation types over time, for the different data types used. All three sampled vegetation types (wheat, isolated weed plants and permanent grassland) were allowed to grow unhindered (no mowing during the study time). The isolated weed plants were initially surrounded by bare soil, but continued to grow in between emerging maize rows in May. During the months of April and May, the weed plants were flowering. The wheat was in the first growth stages after emergence during the February flights and although reproductive structures had formed by May, ripening did not yet start. As such, NDVI values of all studied vegetation types were expected to only rise (moderately) for each subsequent acquisition time. This trend showed up only in the true narrowband multispectral orthomosaics. The trends for CIR-based imagery were widely varying: NDVI based on both RAW and JPEG DN only increased for wheat, but decreased over time for isolated weed plants and permanent grassland. Calibrating the RAW-based orthomosaic DN based on images of the MicaSense reflectance calibration panel improved the trends by showing a steeper increase for wheat and a slight increase for isolated weeds between February and April, more in agreement with the narrowband multispectral data. However, NDVI values for permanent grassland based on calibrated RAW orthomosaics still

showed a decrease, although less steeply, showing that this calibration attempt was unsuccessful. This again suggests that spectral contamination in CIR imagery limits the use even of the RAW data type in multitemporal monitoring. Additional attempts to decrease the spectral contamination by subtracting the RAW blue pixel DN (NIR) from the red DN prior to calibrating or calculating the NDVI as suggested by Verhoeven (2009) actually resulted in worse correlations with ground based NDVI measurements at any time and did not improve the trends over time. This suggests that contamination of the red edge in the red band, as apparent from figure 1 and which is not solved by subtracting the NIR from the red DN, is an equally important degrading factor in spectral data quality as the NIR contamination.

By looking at the evolution of spectral profiles over time (figure 4, bottom row), a better understanding of the NDVI trends and the importance of spectral contamination over spatial resolution can be obtained. For both wheat and isolated weed patches, the February narrowband multispectral profiles deviate only subtly from a bare soil profile, with only a marginal decrease in the red band suggestive of photosynthetic activity in an otherwise linearly increasing profile. The ground pixel size of RAW CIR data was half the ground pixel size of the true narrowband multispectral data and hence more pure (unmixed) pixels can be sampled from isolated plants surrounded by bare soil, such as weeds and emerging wheat. Regardless, much more confusion is apparent from the RAW spectral profiles, with both February and April profiles of weed plants as well as the April profile of wheat characterized by higher DN in red than in green, unrepresentative of healthy growth. For wheat and grass, based on the narrowband multispectral profiles, April and May are characteristic of more photosynthetic activity and healthy growth when compared to February, with decreasing blue and red DN and sharply increasing NIR. For weed plants, although red and blue DN also increased due to the onset of flowering, there was still a sharp rise of NIR over time. Conversely, none of the RAW profiles showed any change in general pattern from February to April, again despite better (more pure) spatial sampling.

It should be noted that while the previous evaluations are mostly based on the NDVI in the present study, the availability of two more bands on the MicaSense as compared to the CIR camera, blue and red edge, would allow for additional information on chlorophyll, further complementing information on crop vigor and health.

Stability of the correlation between UAS-based NDVI and ground based NDVI measurements was evaluated using the linear trend line equations of the February results for each data type [CIR JPEG (5), CIR RAW (6) and true narrowband multispectral (7)] as a model to predict GreenSeeker NDVI values at later dates, using UAS-based NDVI values for those dates as input.

$$NDVI(GS, t2) = \frac{NDVI(UAS, t2) - 0.426}{0.2696} \quad (5)$$

$$NDVI(GS, t2) = \frac{NDVI(UAS, t2) - 0.2029}{0.3945} \quad (6)$$

$$NDVI(GS, t2) = \frac{NDVI(UAS, t2) - 0.1949}{0.9029} \quad (7)$$

The February JPEG model (5) resulted in a RMSE of 0.47 for April, meaning no predictive power of UAS-based NDVI values on ground-based NDVI measurements for April based on the February relation (in April, a UAS-based NDVI of 0.5 could mean either bare soil or very dense vegetation on the ground as measured by the GreenSeeker NDVI). The February RAW model (6) resulted in a RMSE of 0.34 for April which in itself is not much better. However, the average of the model outcome for April was -0.32 (whereas normally errors should be distributed evenly around 0). When deducting the average from the errors, the RMSE dropped to 0.11, meaning much better predictive performance. One hypothesis is that the global shift in errors could point to room for improvement by calibrating RAW DN using a reflectance panel, although figure 4 shows that this approach does not

work on all vegetation types. The February true multispectral model (7) resulted in a RMSE of 0.06 for April and again 0.06 for May, without any indication of global shifts in the errors. This stability of the linear correlation between UAS-based NDVI values and GreenSeeker measurements over time could point to the use of a true narrowband multispectral sensor in repeated in-season mapping as a data source to support variable rate application using existing NDVI-based rules.

The successful reflectance calibration which enables this stable relation over time depends on the calibration method chosen, the way in which the method was performed, the ambient light conditions and the vegetation index studied. Here, pre- and post-flight images of a white reflectance calibration panel were used. This method is quite sensitive to the orientation of the camera and panel at the time of image acquisition in direct sunlight, but works well as long as the procedure is done carefully and the sky is either completely clear (as was the case during the February, April and May flights) or fully overcast during the flight. Onboard upward looking incident light (irradiance) sensors are now more commonly used to deal with changing light conditions, but are also not robust in the case of fast moving small clouds. A situation could occur in which the upward looking sensor sees only clear sky, but the terrain below is covered by a cloud shadow, or vice versa. With the white panel calibration, and due to the normalizing nature of the NDVI, shadows are generally well mitigated on vegetated surfaces in the NDVI map, but other VI maps might be more affected.

Conclusion

In this study, the spectral characteristics of three commonly used data types coming from UAS-borne cameras were evaluated for their potential in remote sensing of crops: out-of-camera JPEG and linear uncompressed RAW from a COTS camera after filter adaptation to enable CIR imaging, and linear uncompressed data from a true narrowband multispectral camera. As the latter type of imaging device has only recently been downsized sufficiently to be mounted in a commercial fixed wing system, enabling systematic mapping of much larger fields compared to a rotary wing UAS, it is important to understand the differences in data characteristics to make informed decisions on what kind of data is best suited for any specific application. The analyses demonstrated an important influence of spectral contamination in both RAW and JPEG data from CIR cameras, next to the data compression artefacts in JPEG data only, even though measures were taken to prevent other degrading influences on the orthomosaic generation such as the adoption of an unusually high forward and sideward overlap (85%) and applying flat field correction with the CIR camera. This shows that while using RAW data can significantly enhance the possibility to retrieve information of field variability on a single day over JPEG imagery, the inherent spectral contamination due to the broad and overlapping bands of a CIR-modified COTS camera still makes it an inferior solution in vigor mapping for precision agriculture applications such as variable rate prescription mapping, especially in a multitemporal context compared to a true narrowband multispectral system. The much better ground sample distance of CIR imagery (resulting in pixels half the size of multispectral pixels), while in theory allowing for more pure target sampling, could not compensate for the spectral confusion due to the overlapping bands. In contrast, a true narrowband multispectral camera showed a very good capability to discern vegetation from bare soil even with small isolated weed plants and in the case of crops in the earliest growth stages after emergence, regardless of the coarser ground pixels. Given a successful reflectance calibration, stability over time is demonstrated, making it a suitable monitoring and prescription mapping tool.

However, the use of much wider looking lenses in combination with high resolution sensors of COTS cameras (resulting in twice the coverage area per flight at half the GSD) also has some important advantages for UAS in agriculture. The ability to get much more vertical detail and better vertical accuracy in surface models at smaller GSDs and in a more productive way (Pauly, 2016) is important in drainage planning, erosion monitoring and when using crop surface models to estimate biomass and yield (Bendig et al., 2014), or in the framework of crop damage assessment following storms. Although not strictly necessary, using CIR imagery for this type of high resolution mapping can help substantially e.g. in assessing flooded areas in row crop fields, or to increase contrasts between bare

soil and vegetation as compared to RGB imagery when performing automated classification and counting. The use of a very high resolution RGB or CIR unmanned system with precise positioning technology such as the Trimble UX5 HP can complement the use of a UAS with a true narrowband multispectral camera such as the Trimble UX5 with Micasense RedEdge, by generating accurately georeferenced maps and models with minimal ground control effort, which can then serve as base maps to reference true narrowband multispectral orthomosaics on in a GIS. The availability of more detailed and accurate 3D surface information can additionally help in interpreting the variability in leaf area index and leaf chlorophyll concentrations derived from true narrowband multispectral imaging.

Acknowledgements

Trimble acknowledges the assistance of Marc De Schepper and Dirk Ryckaert (Assenede, Belgium) for allowing permanent UAS flight operations and ground measurements on their private farm properties. Jack Paris (Paris Geospatial, Clovis, CA) and Jim Quaderer (Trimble Ag, Sunnyvale, CA) are greatly acknowledged for numerous valuable comments and discussions on CIR and multispectral UAS data characteristics and requirements. Peter Cosyn (Trimble UAS, Gent, Belgium) provided feedback on this paper.

References

- Aschbacher, J. & Milagro-Pérez, M. P. (2012). The European earth monitoring (GMES) programme: Status and perspectives. *Remote Sensing of Environment*, 120, 3-8.
- Bendig, J., Bolten, A., Bennertz, S., Broscheit, J., Eichfuss, S. & Bareth, G. (2014). Estimating biomass of barley using crop surface models (CSMs) derived from UAV-based RGB imaging. *Remote Sensing*, 6, 10395-10412.
- Berra, E., Gibson-Poole, S., MacArthur, A., Gaulton, R. & Hamilton, A. (2015). Estimation of the spectral sensitivity functions of un-modified and modified commercial off-the-shelf digital cameras to enable their use as a multispectral imaging system for UAVs. In *The International Archives of the Photogrammetry, Remote Sensing and Spatial Information Sciences*, XL(1-W4), Proceedings of the International Conference on Unmanned Aerial Vehicles in Geomatics, 207-215.
- Coffin, D. (2008). Decoding raw digital photos in Linux. Online software publication. <https://www.cybercom.net/~dcoffin/dcraw>. Accessed 28 June 2016.
- d'Oleire-Oltmanns, S., Marzolf, I., Peter, K. D. & Ries J. B. (2012). Unmanned aerial vehicle (UAV) for monitoring soil erosion in Morocco. *Remote Sensing*, 4, 3390-3416.
- Fang, S., Tang, W., Peng, Y., Gong, Y., Dai, C., Chai, R. & Liu, K. (2016). Remote estimation of vegetation fraction and flower fraction in oilseed rape with unmanned aerial vehicle data. *Remote Sensing*, 8, 416-434.
- Gómez-Candón, D., De Castro A. I. & López-Granados, F. (2014). Assessing the accuracy of mosaics from unmanned aerial vehicle (UAV) imagery for precision agriculture purposes in wheat. *Precision Agriculture*, 15, 44-56.
- Hunt, E. R. Jr., Hively, W. D., Fujikawa, S. J., Linden, D. S., Daughtry, C. S. T. & McCarty, G. W. (2010). Acquisition of NIR-Green-Blue digital photographs from unmanned aircraft for crop monitoring. *Remote Sensing*, 2, 290-305.
- Lebourgeois, V., Bégué, A., Labbé, S., Houllès, M. & Martiné, J. F. (2012). A light-weight multi-spectral aerial imaging system for nitrogen crop monitoring. *Precision Agriculture*, 13, 525-541.
- Lebourgeois, V., Bégué, A., Labbé, S., Mallavan, B., Prévot, L. & Roux, B. (2008). Can commercial digital cameras be used as multispectral sensors? A crop monitoring test. *Sensors*, 8, 7300-7322.
- Lelong, C. C. D., Burger, P., Jubelin, G., Roux, B., Labbé, S. & Baret, F. (2008). Assessment of unmanned aerial vehicles imagery for quantitative monitoring of wheat crop in small plots. *Sensors*, 8, 3557-3585.
- Mulla, D. J. (2013). Twenty five years of remote sensing in precision agriculture: Key advances and remaining knowledge gaps. *Biosystems Engineering*, 114, 358-371.
- Pauly, K. (2014). Applying conventional vegetation vigor indices to UAS-derived orthomosaics: Issues and considerations. In *Proceedings of the 12th International Conference on Precision Agriculture*. <https://www.ispag.org/icpa/Proceedings>. Accessed 28 June 2016.
- Pauly, K. (2016). Trimble UX5 HP – Increasing your productivity. White Paper. Trimble Navigation Ltd., Sunnyvale, CA, USA. http://uas.trimble.com/sites/default/files/downloads/trimbleux5hp_whitepaper.pdf. Accessed 28 June 2016.
- Peña, J. M., Torres-Sánchez, J., Serrano-Pérez, A., de Castro A. I. & López-Granados F. (2015). Quantifying efficacy and limits of unmanned aerial vehicle (UAV) technology for weed seedling detection as affected by sensor resolution. *Sensors*, 15, 5609-5626.
- Rabatel, G., Gorretta, N. & Labbé, S. (2014). Getting simultaneous red and near-infrared band data from a single digital camera for plant monitoring applications: theoretical and practical study. *Biosystems Engineering*, 117(1), 2-14.
- Rasmussen, J., Ntakos, G., Nielsen, J., Svenggaard, J., Poulsen, R. N. & Christensen, S. (2016). Are vegetation indices

- derived from consumer-grade cameras mounted on UAVs sufficiently reliable for assessing experimental plots? *European Journal of Agronomy*, 74, 75-92.
- Tyc, G., Tulip, J., Schulten, D., Krischke, M. & Oxfort, M. (2005). The RapidEye mission design. *Acta Astronautica*, 56, 213-219.
- Verhoeven, G. J. J. (2010). It's all about the format – unleashing the power of RAW aerial photography. *International Journal of Remote Sensing*, 31(8), 2009-2042.
- Verhoeven, G. J. J., Smet, P. F., Poelman, D. & Vermeulen, F. (2009). Spectral characterization of a digital still camera's NIR modification to enhance archaeological observation. *IEEE Transactions on Geoscience and Remote Sensing*, 47(10), 3456-3468.
- Wezel, A., Casargrande, M., Celette, F., Vian, J.-F., Ferrer, A. & Peigné, J. (2014). Agroecological practices for sustainable agriculture. A review. *Agronomy for Sustainable Development*, 34, 1-20.
- Zarco-Tejada, P. J., Diaz-Varela, R., Angileri, V. & Loudjani, P. (2014b). Tree height quantification using very high resolution imagery acquired from an unmanned aerial vehicle (UAV) and automatic 3D photo-reconstruction methods. *European Journal of Agronomy*, 55, 89-99.
- Zarco-Tejada, P. J., Hubbard, N. & Loudjani P. (2014a). Precision agriculture: an opportunity for EU farmers – Potential support with the CAP 2014-2020. Study. Directorate-General for Internal Policies, European Parliament. [http://www.europarl.europa.eu/RegData/etudes/notes/join/2014/529049/IPOL-AGRI_NT\(2014\)529049_EN.pdf](http://www.europarl.europa.eu/RegData/etudes/notes/join/2014/529049/IPOL-AGRI_NT(2014)529049_EN.pdf). Accessed 28 June 2016.
- Zhang, C. & Kovacs, J. M. (2012). The application of small unmanned aerial systems for precision agriculture: a review. *Precision Agriculture*, 13, 693-712.